e-Navi

Available online at http://www.e-navigation.kr/
e-Navigation Journal

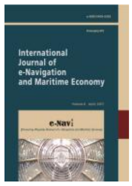

Original article

Bidirectional Dynamic Responses and Feature Sensitivity to Variations in Crack Elevation in an Offshore Wind Turbine Tower under Combined Stochastic Wind–Wave Loading

Kexin Zhang[a], Zhuoyi Yang[b*], Jingkai Bi[c], Pengfei Ge[d], Jiaxin Zhang[e]

[a] School of Naval Architecture and Port Engineering, Shandong Jiaotong University, Weihai 264209, China, 2604882862@qq.com

[b*] School of Naval Architecture and Port Engineering, Shandong Jiaotong University, Weihai 264209, China, 19952115921@163.com, Corresponding Author

[c] School of Naval Architecture and Port Engineering, Shandong Jiaotong University, Weihai 264209, China, 1322768318@qq.com

[d] School of Naval Architecture and Port Engineering, Shandong Jiaotong University, Weihai 264209, China, 3380948128@qq.com

[e] School of Naval Architecture and Port Engineering, Shandong Jiaotong University, Weihai 264209, China, 672554352@qq.com

Abstract

Conventional amplitude-based indicators may be insufficient to characterise the effects of varying crack elevation in offshore wind turbine towers. To address this limitation, a bidirectional multi-feature sensitivity analysis was conducted using a finite element model based on the NREL 5 MW reference wind turbine. Transient dynamic analyses were performed in ANSYS under combined stochastic wind–wave loading. One intact case and five cracked cases with identical crack dimensions but different elevations were considered. Acceleration responses in the X and Y directions were extracted at eight measurement points. The root-mean-square value, peak absolute acceleration, dominant frequency, and frequency-band energy indices were calculated, and their sensitivities to variations in crack elevation were quantified using the absolute relative change with respect to the intact case. Under the adopted loading conditions, the X-direction response exhibited a larger overall amplitude. However, the RMS and frequency-band energy indices exhibited higher relative sensitivities in the Y direction, whereas the peak-value sensitivity was higher in the X direction. No detectable change in dominant frequency was observed at the adopted frequency resolution. Among the investigated features, the frequency-band energy in the 0–0.05 Hz band exhibited the highest sensitivity in both directions. Among the eight candidate measurement points, P1 showed the highest sensitivity under the considered loading and crack cases, and the sensitivity generally decreased with increasing measurement height. These findings provide a basis for damage-sensitive feature selection and sensor-layout optimisation in crack monitoring of offshore wind turbine towers.

Keywords: Forecasting production, Time Series Regression Model, Holt-Winters, Uncertainty Theory, exported Catfish, Mekong Delta.

https://doi.org/10.52820/j.enavi.2026.26.010

1. Introduction

Driven by the global energy transition and decarbonisation targets, offshore wind turbines are being developed with larger capacities and deployed in increasingly deep waters. During long-term operation, offshore wind turbine towers are subjected to combined wind, wave, current, and operational loads, which may lead to fatigue cracking, localised stiffness degradation, and changes in structural dynamic characteristics. A clear understanding of the dynamic responses associated with tower cracking under realistic environmental loading is therefore essential for structural health monitoring and damage detection.

Previous studies have mainly focused on vibration-based damage identification, global structural responses, and the dynamic behaviour of offshore wind turbine support structures. Yan et al. [1] demonstrated that structural damage alters stiffness and consequently affects natural frequencies, mode shapes, and vibration responses. Ran et al. [2] showed that the identification of damage-sensitive frequency bands can improve damage-detection performance. For offshore wind turbine structures, Xu et al. [3], Chen et al. [4], and Li et al. [5] investigated dynamic responses and fatigue-damage distributions under earthquake excitation, coupled environmental loading, and combined wind–wave effects, respectively. Van Vondelen et al. [6] and Cheng et al. [7] further examined the effects of operating and foundation conditions on structural dynamic characteristics. These studies provide an important basis for the dynamic analysis and damage identification of offshore wind turbines.

Despite these advances, most existing studies have concentrated on global dynamic responses, modal parameters, and fatigue-life assessment, whereas the effects of varying crack elevation on bidirectional response characteristics remain insufficiently understood. Tian et al. [8] showed that crack number and crack interaction can significantly affect crack propagation and structural residual life, further highlighting the complexity of crack-related problems. Meanwhile, data-driven and deep learning methods have provided effective tools for feature extraction and damage classification under complex operating conditions [9–11]. However, their performance still depends strongly on the selection of damage-sensitive features and a clear understanding of the underlying structural response mechanisms [12]. In particular, the influence of crack-elevation variation on X/Y acceleration responses and frequency-band energy redistribution under combined stochastic wind–wave loading has not been adequately clarified. This limits the effective selection of damage-sensitive features and the development of reliable crack-identification models.

To address these gaps, this study investigates the bidirectional dynamic responses and feature sensitivities of an offshore wind turbine tower with varying crack elevations under combined stochastic wind–wave loading. The main contributions are as follows:

(1) A bidirectional multi-feature sensitivity framework is developed to evaluate the effects of crack-elevation variation on the X/Y acceleration responses of an offshore wind turbine tower.

(2) The relationship between absolute response magnitude and relative damage sensitivity is clarified, showing that the direction with the larger vibration amplitude does not necessarily exhibit higher sensitivity to variations in crack elevation.

(3) The sensitivities of the root-mean-square value, peak absolute acceleration, dominant frequency, and frequency-band energy are systematically compared, and the most sensitive feature and measurement point are identified for the loading and crack cases considered in this study.

A finite element model based on the NREL 5 MW reference wind turbine was established to achieve these objectives. One intact case and five cracked cases with identical crack dimensions but different elevations were analysed under combined stochastic wind–wave loading. The X/Y acceleration responses at eight measurement points were evaluated using time- and frequency-domain features, and their sensitivities were quantified using the absolute relative change with respect to the intact case.

2. Finite element modelling of the offshore wind turbine tower and load application

2.1 Basic specifications of the NREL 5 MW reference wind turbine

The finite element model developed in this study was based on the NREL 5 MW reference wind turbine. The tower of the NREL 5 MW wind turbine is conical, with a base diameter of 6 m and a thickness of 0.027 m, and a top diameter of 3.87 m and a thickness of 0.019 m. It is constructed from Q235 steel, with a Young's modulus of 210 GPa and a shear modulus of 80.8 GPa. An equivalent density of 8500 kg/m³ was adopted in the finite element model, instead of the nominal Q235 density of 7850 kg/m³, to account for the effects of paint, bolts, welds and flanges on the tower [13]. As this study focuses on relative dynamic response differences and feature extraction under different crack-elevation cases, rather than the precise prediction of local peak stresses, the nacelle, hub and rotor system were simplified as equivalent eccentric mass blocks that reproduced the same total mass and overturning moment acting on the tower. The model employs a tetrahedral mesh with local refinement in the vicinity of the cracks to enhance the accuracy of local response analysis and meet the requirements for subsequent dynamic response analysis and feature extraction. The relevant parameters are shown in Table 1.

Table 1 Main parameters of the offshore wind turbine and the finite element model

Parameter	Value
Rated power	5 MW
Hub height	90 m
Yaw-axis height	87.6 m
Total tower height	126 m
Monopile diameter	6 m
Submerged length	20 m
Embedded-soil length	36 m
Nacelle mass	240 t
Rotor mass	110 t
Equivalent top mass	350 t
Rated wind speed	11.4 m/s
Cut-in / cut-out wind speed	3 m/s / 25 m/s

2.2 Establishment of the finite element model

A three-dimensional geometric model of the offshore wind turbine tower was established in SolidWorks and imported into ANSYS for finite element analysis. The model comprises the main tower body, a 20-metre submerged section, a 36-m section embedded in the seabed soil, and the equivalent section comprising the top nacelle, hub and rotor. Prior to the calculations, a comparison was made between three mesh densities. The results indicate that the relative error in the acceleration response characteristics is less than 3%, demonstrating that the meshing strategy adopted is reliable. The mesh definition for the tower and the crack region is shown in Figure 1.

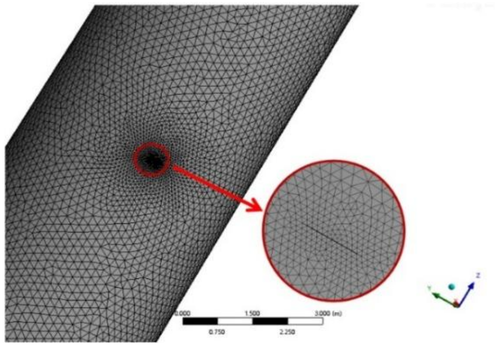

Fig 1 Mesh generation for the tower shell and the crack region

2.3 Application of wind and wave loads

To simulate the service loading conditions experienced by offshore wind turbine towers in actual operating environments, this paper applies combined wind and wave time-history loads to a finite element model. The wind loads utilise time-history data for turbulent wind loads extracted from GH Bladed. A 1000-s load history at a wind speed of 16 m/s was selected, with a time step of 1 second; the improved von Karman turbulence model was adopted. Typical time-history curves for wind and wave loads are shown in Figures 2 and 3, respectively.

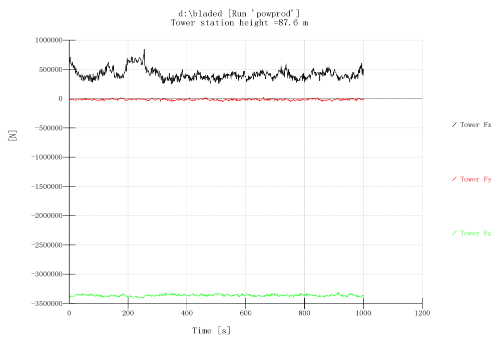

(a) Time history diagram of force loads at the top of the tower

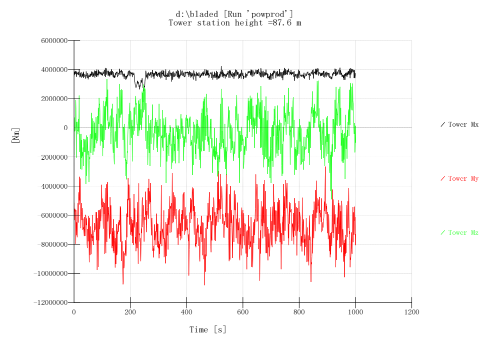

(b) Time history diagram of the moment load at the top of the tower

Fig 2 Typical wind-load time histories

Wave loads act primarily on the submerged tower section. Taking into account their distribution characteristics along the height, this paper divides the 20-metre submerged section of the tower into four zones. Based on the wave time-history loads for each zone, these loads were applied to the corresponding surface regions using the Remote Force option in ANSYS to approximate their spatial distribution characteristics. Due to the lack of detailed soil parameters, the equivalent pile method is adopted, with a fixed constraint applied at a depth of six times the pile diameter below the mudline to approximate the pile-soil interaction[14]. Given that aerodynamic loads are primarily transmitted to the tower through the tower top, wind loads are equivalently applied to a reference point at the tower top in this study. Wind and wave loads together constitute a combined wind-wave excitation scenario. Compared with single-load analysis, this method can more reasonably reflect the complex stress conditions encountered by offshore wind turbines in their actual operating environment.

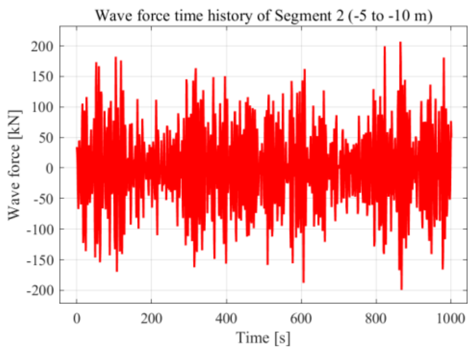

Fig 3 Wave force time history in the -5 to -10 m segment

2.4 Modal analysis of the tower

After the finite element model had been established, the Block Lanczos method was used to extract the first six natural frequencies of the wind turbine tower, as shown in Table 2. Owing to the approximately axisymmetric tower structure, the first and second, third and fourth, and fifth and sixth natural frequencies are very close to each other.

Table.2 First six natural frequencies of the tower

Modal order	Natural frequency/Hz
1	0.19941
2	0.20034
3	1.2465
4	1.2556
5	3.3452
6	3.3693

2.5 Transient dynamic analysis settings

A structural dynamic response analysis under combined wind and wave loads was conducted using the ANSYS Transient Dynamics module, with a total analysis duration of 1000 s and a time step of 1 s. To minimise the impact of the initial transient phase on the statistical results, subsequent feature extraction was performed using the relatively stable response segment obtained after removing the initial transient part. The output results included the acceleration response time histories in the X and Y directions at eight measurement points, which were used for subsequent feature extraction and feature sensitivity analysis.

3. Crack cases and arrangement of measurement points

3.1 Crack case settings

To analyse the effect of variations in crack elevation on the dynamic response of the tower structure, this paper defines one intact case and five cracked cases. All cracks were defined as circumferential cracks with identical dimensions, with the aim of keeping the crack size constant and isolating the influence of crack-elevation variation on the structural dynamic response characteristics; this configuration balances the need for discernible local stiffness reduction with the feasibility of numerical analysis. The specific cases are shown in Table 3.

Table.3 Crack cases

Case	Crack elevation/ m	Crack parameters
T0	/	No crack damage
T1	8.76 m	Length 200 mm, width 2 mm, depth 35%t
T2	17.52 m	Length 200 mm, width 2 mm, depth 35%t
T3	26.28 m	Length 200 mm, width 2 mm, depth 35%t

T4	35.04 m	Length 200 mm, width 2 mm, depth 35%t
T5	43.8 m	Length 200 mm, width 2 mm, depth 35%t

3.2 Arrangement of measurement points

To determine the distribution of structural dynamic responses along the height of the tower, eight measurement points were arranged along the axial direction of the tower shell at heights of 5 m, 12 m, 20 m, 28 m, 36 m, 44 m, 60 m and 80 m, as shown in Table 4. This arrangement covers the lower, middle and upper regions of the tower shell, and is well suited to characterising the propagation and attenuation patterns of crack-induced vibrations along the height.

Table.4 Arrangement of measurement points

Point	Height / m	Point location
P1	5	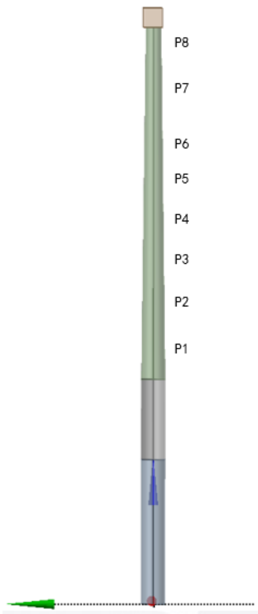
P2	12	
P3	20	
P4	28	
P5	36	
P6	44	
P7	60	
P8	80	

4. Feature extraction methods and bidirectional sensitivity analysis

4.1 Feature extraction methods

To analyse variations in the dynamic response of the offshore wind turbine tower under different crack-elevation cases, this paper extracts time-domain and frequency-domain characteristic parameters from the acceleration time histories at measurement points in the X and Y directions. Feature sensitivity indices were then established using the intact case as the reference, to evaluate the ability of different measurement points and characteristics to characterise crack damage.

The root-mean-square (RMS) value was used to quantify the overall magnitude of the acceleration response. A larger RMS value indicates a greater overall vibration magnitude.

$$\mathrm{RMS} = \sqrt{\frac{1}{N}\sum_{i=1}^{N} a_i^2} \qquad (1)$$

In the equation, a_i represents the acceleration value at the ith sampling point, and N represents the total number of sampling points.

The peak absolute acceleration is used to characterise the maximum amplitude of an acceleration signal, and is expressed as

$$\mathrm{Peak} = \max(|a_i|) \qquad (2)$$

The peak absolute acceleration reflects the instantaneous extreme response amplitude, but it is relatively sensitive to transient fluctuations.

To obtain the structural frequency-distribution characteristics, a fast Fourier transform (FFT) is performed on the acceleration time histories to obtain the single-sided amplitude spectrum, from which the dominant frequency and band-energy features are extracted.

The dominant frequency is defined as the frequency corresponding to the maximum amplitude in the single-sided spectrum excluding the zero-frequency component, representing the dominant frequency component in the structural response. This feature can be used to reflect the change in overall structural dynamic characteristics.

To analyse the variation in energy distribution across different frequency intervals, the frequency domain is divided into four bands, denoted by B1, B2, B3 and B4.

B_1: 0–0.05 Hz;

B_2: 0.05–0.10 Hz;

B_3: 0.10–0.20 Hz;

B_4: 0.20–0.50 Hz.

Because the output time step is 1 s, the corresponding sampling frequency is 1 Hz and the Nyquist frequency is 0.5 Hz. Therefore, the frequency-domain analysis range is limited to 0-0.5 Hz. Combined with the low-frequency response characteristics of the tower, this range is divided into four frequency bands to compare the spectral-energy redistribution under different crack-elevation cases.

The energy within the kth band is defined as

$$E_k = \sum_{f_j \in B_k} A(f_j)^2 \qquad (3)$$

In the equation, $A(f_j)$ represents the amplitude of the one-sided amplitude spectrum at frequency f_j, and Bk denotes the k th frequency band. Frequency-band energy can characterise the redistribution of spectral energy caused by cracks.

To compare the degree of change in each feature parameter under different crack cases relative to the intact case, the absolute relative change was adopted as the sensitivity index and is defined as

$$S = \left| \frac{F_d - F_0}{F_0} \right| \qquad (4)$$

In the equation, F_0 represents the value of a characteristic parameter in intact cases, F_d represents the corresponding value of the characteristic parameter in cracked cases, and S is an indicator of the sensitivity of that characteristic to variations in crack elevation. The larger the value of S, the more sensitive the characteristic is to variations in crack elevation.

4.2 Sensitivity analysis of X/Y bidirectional features

To compare the ability of the X- and Y-direction responses to characterise variation in crack elevation, RMS, peak absolute acceleration, dominant frequency, and frequency-band energy were extracted from the acceleration responses at eight measurement points. The relative change rate of each damaged case was calculated with respect to the intact case. The average bidirectional sensitivities are presented in Fig 4, while Fig 5 further compares the RMS responses in the X and Y directions at measurement point P8. As shown in Table 5, the absolute relative changes of dominant frequency in both directions are 0, indicating that the dominant frequency remains nearly unchanged under different crack-elevation cases and is therefore insensitive to variation in crack elevation. In contrast, frequency-band energy shows a much clearer response, among which the low-frequency band energy E_1 is the most sensitive feature. Its feature sensitivity is 2.3283×10^{-2} in the X direction and 1.8024×10^{-1} in the Y direction, both significantly higher than those of RMS, peak absolute acceleration, and the other band-energy features. This suggests that variation in crack elevation is more readily reflected in the redistribution of low-frequency energy than in a shift of dominant frequency.

Table 5 Average sensitivity statistics of X/Y bidirectional features

Direction	RMS	Peak
X	3.316×10^{-5}	3.0244×10^{-4}
Y	5.6146×10^{-4}	1.1422×10^{-4}

Direction	Dominant frequency	E1	E2
X	0	2.3283×10^{-2}	2.4033×10^{-3}
Y	0	1.8024×10^{-1}	2.3708×10^{-2}

Direction	E3	E4
X	6.9138×10^{-5}	9.4698×10^{-4}
Y	1.0634×10^{-3}	3.7612×10^{-3}

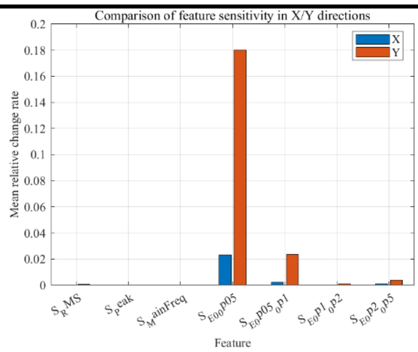

Fig 4 Comparison of X/Y bidirectional feature sensitivities

Figure 4 and Table 5 reveal a clear distinction between response magnitude and damage sensitivity. Although the absolute acceleration response is dominated by the X direction, the relative sensitivities of the RMS and frequency-band energy indices are generally higher in the Y direction. Specifically, the Y-to-X sensitivity ratios are approximately 16.9 for RMS and 7.7, 9.9, 15.4, and 4.0 for the E1–E4 frequency-band energy indices, respectively. In particular, the sensitivity of E1 in the Y direction is approximately 7.7 times that in the X direction. However, this directional tendency is not observed for all features: the peak-value sensitivity in the Y direction is only approximately 0.38 times that in the

X direction, while no detectable change in dominant frequency is observed in either direction.

These results demonstrate that the direction of the largest response amplitude does not necessarily coincide with the direction of the highest damage sensitivity. The larger X-direction amplitude mainly reflects the dominant global vibration response induced by the adopted wind–wave loading. By contrast, the sensitivity index is normalised by the corresponding intact-state feature value and therefore describes the proportional disturbance caused by crack-elevation variation. Although the Y-direction response has a smaller absolute magnitude, its RMS and frequency-band energy indices undergo larger relative changes, making these features more responsive to local stiffness perturbations under the considered conditions.

The comparison of RMS values across the various measurement points reveals that the response amplitude in the X direction is generally significantly greater than that in the Y direction; under combined wind and wave loads, the tower's primary vibration response is concentrated in the X direction. Since P8 is located in the upper section of the tower, it can clearly reflect directional differences in the global response amplitude. Therefore, P8 was selected for the X/Y RMS comparison shown in Figure 5.

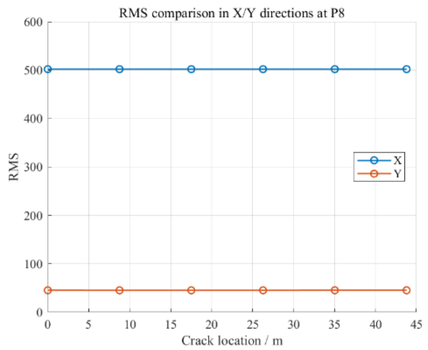

Fig 5 Comparison of RMS values in the X and Y directions at measurement point P8

Figure 5 compares the absolute RMS responses in the X and Y directions and therefore characterises the directional difference in global vibration magnitude. It should not be interpreted directly as a comparison of damage sensitivity. The substantially larger X-direction RMS indicates that the global response is dominated by the X direction under the adopted loading conditions. However, the variation of the RMS value among the different crack-elevation cases is relatively limited. This confirms that a large absolute response does not necessarily provide strong discrimination among crack-elevation cases. In contrast, the relative-change analysis in Table 5 shows that the Y-direction RMS, although smaller in absolute magnitude, is proportionally more sensitive to crack-elevation variation.

Among the features investigated in this study, the frequency-band energy index E1 exhibited the highest sensitivity in both directions. Its sensitivity was 2.3283×10^{-2} in the X direction and 1.8024×10^{-1} in the Y direction, with the latter being approximately 7.7 times the former.

Further analysis of the low-frequency energy sensitivity at each measurement point shows that P1 is the most sensitive point in both the X and Y directions, and the sensitivity generally decreases from P1 to P8. This indicates that lower measurement points are more sensitive to variation in crack elevation, whereas the sensitivity of higher points gradually weakens.

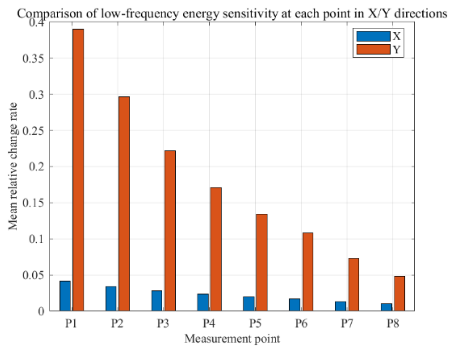

Fig 6 Comparison of low-frequency energy sensitivity at each measurement point in the X/Y directions

As shown in Figure 6, the low-frequency energy sensitivity reaches its maximum at P1 in both directions and then decreases with increasing measurement height. This trend is consistent with the crack-elevation cases considered in this study, which are distributed mainly in the lower and middle regions of the tower. This tendency may be associated with the larger bending moment and curvature in the lower part of the tower, as well as the relative proximity of the lower measurement points to the investigated crack elevations. Further modal-strain-energy analysis would be required to fully verify this mechanism. Consequently, in sensor layout optimisation, priority should be given to lower tower locations, especially near P1, to improve the identification of variation in crack elevation.

To further illustrate the bidirectional response characteristics of the most sensitive measurement point, the lowest-frequency band energy curves in the X and Y directions at measurement point P1 were plotted against crack elevation, as shown in Figure. 7.

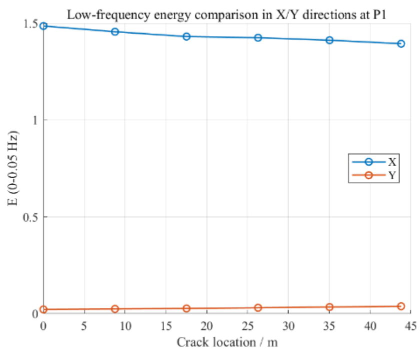

Fig 7 Variation of low-frequency energy with crack location at measurement point P1 in the X/Y directions

The frequency-band energy index E1 at P1 varied with crack elevation in both directions, with more pronounced changes observed in the Y direction. This result is consistent with the average sensitivities reported in Table 5 and Fig. 4, further confirming the higher sensitivity of the Y-direction E1 index to variations in crack elevation. The observed changes may be attributed to the redistribution of local stiffness caused by varying crack elevation, which subsequently affects the frequency-band energy distribution of the tower response.

5. Discussion

The results indicate that variations in crack elevation are mainly reflected in the redistribution of the response components in the 0–0.05 Hz band rather than in a detectable shift in dominant frequency. Under the adopted loading conditions, the overall acceleration amplitude was larger in the X direction. However, the RMS and frequency-band energy indices exhibited higher relative sensitivities in the Y direction, whereas the peak-value sensitivity was higher in the X direction. Therefore, the direction with the largest absolute response does not necessarily coincide with the direction exhibiting the highest damage sensitivity.

The difference between the X/Y response amplitudes and their sensitivities may be attributed to the combined effects of loading direction, intact-state baseline response, and crack-induced stiffness redistribution. The dominant environmental loading component produced a larger global response in the X direction. By contrast, the sensitivity index was normalised by the corresponding intact-state feature value. Consequently, the smaller Y-direction baseline may partly contribute to the larger relative changes observed in its RMS and frequency-band energy indices. The peak-value feature did not follow the same directional tendency and may be more strongly influenced by isolated transient extremes. These results support the joint use of X/Y bidirectional features rather than reliance on the response amplitude from a single direction.

It should be emphasised that the observed directional sensitivity depends on the loading direction, crack orientation, circumferential crack position, and adopted normalisation method. Therefore, the results do not imply that the Y direction is universally more sensitive for all offshore wind turbine towers. Instead, they demonstrate that the dominant vibration direction and the most damage-sensitive direction may differ under a specific loading and damage configuration.

6. Conclusions

This study established a finite element model of an offshore wind turbine tower with varying crack elevations under combined stochastic wind–wave loading, and performed feature extraction and sensitivity analysis on the X/Y acceleration responses at eight measurement points. The main conclusions are as follows:

(1) Under the adopted wind–wave loading conditions, the overall acceleration response is dominated by the X direction. However, the RMS and frequency-band energy indices exhibit higher relative sensitivity in the Y direction, whereas the peak-value sensitivity is higher in the X direction. This result confirms that the direction of the largest response amplitude does not necessarily coincide with the direction of the highest damage sensitivity;

(2) The dominant frequency remains largely unchanged under different crack-elevation cases and is therefore unsuitable as the primary feature for characterising variation in crack elevation under the present conditions;

(3) Under the considered loading and crack cases, the frequency-band energy index E1 exhibited the highest sensitivity in both directions and was the most sensitive feature among those investigated;

(4) Lower measurement points are more sensitive to

variations in crack elevation; under the conditions of this study, P1 is the most sensitive measurement point, and the sensitivity of measurement points generally decreases with increasing height.

These findings provide guidance for damage-sensitive feature selection, measurement-point layout optimisation and subsequent crack-identification studies for offshore wind turbine towers.

References

[1]Yan, Y.J., Cheng, L., Wu, Z.Y., et al.: 'Development in vibration-based structural damage detection technique', Mech. Syst. Signal Process., 2007, 21, (5), pp. 2198–2211.

[2]Ran, Z.H., Miao, S., Qu, J.T.: 'Extraction of structure-sensitive frequency bands and its application in damage identification' (in Chinese), Highway Engineering, 2010, 35, (1), pp. 67–71.

[3]Xu, M., Au, F.T.K., Wang, S., et al.: 'Dynamic response analysis of a real-world operating offshore wind turbine under earthquake excitations', Ocean Eng., 2022, 266, p. 112791.

[4]Chen, Z., Chen, F., Liu, H., et al.: 'Dynamic response of offshore wind turbine monopile foundations in layered soils under wind, wave and earthquake actions', Appl. Ocean Res., 2025, 162, p. 104728.

[5]Li, B., Shi, H., Rong, K., et al.: 'Fatigue life analysis of offshore wind turbine under the combined wind and wave loadings considering full-directional wind inflow', Ocean Eng., 2023, 281, p. 114719.

[6]van Vondelen, A.A.W., Iliopoulos, A., Navalkar, S.T., et al.: 'Modal analysis of an operational offshore wind turbine using enhanced Kalman filter-based subspace identification', Wind Energy, 2023, 26, (9), pp. 923–945.

[7]Cheng, X., Xing, J., Wang, G., et al.: 'Numerical investigation on rotation accumulation and natural frequency degradation for offshore wind turbine in clays', Ocean Eng., 2025, 315, p. 119761.

[8]Tian, J., Li, X., Li, F.: 'Research on fatigue crack growth life of offshore wind turbine towers with double cracks in extreme environments', J. Offshore Mech. Arct. Eng., 2025, 147, (5), p. 052001.

[9]Cha Y J, Ali R, Lewis J, et al. Deep learning-based structural health monitoring[J]. Automation in Construction, 2024, 161: 105328.

[10]Triviño H, Feijóo M C, Lugmania H, et al. Damage detection and localization at the jacket support of an offshore wind turbine using transformer models[J]. Structural Control and Health Monitoring, 2023, 2023: 6646599.

[11]Song F, Han Y, Heath A W, et al. Structural damage detection of floating offshore wind turbine blades based on Conv1d-GRU-MHA network[J]. Engineering Failure Analysis, 2024, 166: 108896.

[12]Lee Y, Kim H, Min S, et al. Structural damage detection using deep learning and FE model updating techniques[J]. Scientific Reports, 2023, 13: 18694.

[13]Jonkman, J., Butterfield, S., Musial, W., Scott, G.: 'Definition of a 5-MW Reference Wind Turbine for Offshore System Development' (NREL, 2009), NREL/TP-500-38060.

[14]Song, Y., Lu, D., Zuo, J., Wang, W., Li, X.: 'Dynamic characteristics of monopile offshore wind turbine with different equivalent pile foundation boundaries under winds, waves and earthquakes', Applied Ocean Research, 154 (2025), 104391.

Received **23 April 2026**

1st Revised **25 June 2026**

Accepted **30 June 2026**